Bimetallic platinum-rhodium nanocomposites for dimethylamine borane dehydrogenation: An Experimental and Density Functional Theory Study

Oznur Alptekin[a≅], Betul Sen[b≅], Hilal Acidereli[b], Umran Ercetin*[a], Mehmet Ferdi Fellah[c], Fatih Sen*[b]

[a]Department of Mechanical Engineering, Faculty of Engineering, Dumlupınar University, Evliya Çelebi Campus,43100 Kütahya, Turkey

[b]Sen Research Group, Department of Biochemistry, Faculty of Art and Science, Dumlupınar University, Evliya Çelebi Campus,43100 Kütahya, Turkey

[c]Department of Chemical Engineering, Bursa Technical University, Mimar Sinan Campus, 16310, Bursa, Turkey

≅*These authors contributed equally to this work.*

**Corresponding author.*

(Corresponding authors: umran.ercetin@dpu.edu.tr, fatih.sen@dpu.edu.tr)

Synthesis of graphene oxide (GO)

Graphene oxide (GO) was synthesized from graphite powder using a modified Hummer's method. In brief, 1 g of graphite and 0.5 g of sodium nitrate were mixed followed by the addition of 23 mL of conc. sulphuric acid under constant stirring. After 1 h, 3 g of $KMnO_4$ was added gradually to the above solution while keeping the temperature less than 20 °C to prevent overheating and explosion. The mixture was stirred at 35 °C for 12 h and the resulting solution was diluted by adding 500 mL of water under vigorous stirring. To ensure the completion of the reaction with $KMnO_4$, the suspension was further treated with 30 % H_2O_2

solution (5 mL). The resulting mixture was washed with HCl and H_2O respectively, followed by filtration and drying, graphene oxide sheets were thus obtained [1].

Computational Method

The graphene oxide (GO) cluster used for calculations has 40 Carbon atoms and 10 Oxygen atoms, which means there are 10 epoxy groups. The structure of GO used in this study is represented in Figure S2. Dangling bonds of the C atoms have been saturated with H atoms in order to result in the neutral cluster. The very similar structure of GO cluster used here has been utilized in a recent theoretical study [2]. One Pt and one Rh atom have been used to obtain PtRh@GO cluster that is to represent the PtRh@GO catalyst. These metal atoms have been located on p1 and p2 points (see Figure S2) on the GO cluster. A similar strategy in order to obtain Pt decorated GO cluster has been utilized during DFT calculations for methane to methanol on platinum-decorated sheets of graphene oxide [2]. Two Pt atoms have been located on some points that are similar to the points used in that study [2].

The geometries were optimized geometrically using equilibrium geometry (EG) calculations and obtain adsorption energies. In the present study, energy difference values include zero-point energy (ZPE) corrections. These energies were calculated using the frequency keyword (freq) in Single Point Energy (SPE) calculations. In addition, vibrational frequency, thermal energy, thermal enthalpy, and thermal free energy values were calculated by SPE calculations at 298 K and atmospheric pressure in Gaussian software [3,4]. These energy values were computed as follows:

$$E = E_{electronic} + ZPE + E_{vibrational} + E_{rotational} + E_{translational} \quad (1)$$

$$H = E + RT \quad (2)$$

$$G = H - TS \quad (3)$$

where E is the sum of the electronic, zero point and thermal energies, H is the sum of the electronic and thermal enthalpies, G is the sum of electronic and thermal free energy, S is the Entropy and T is the temperature used for the vibrational frequency calculations. HOMO and LUMO representations and HOMO/LUMO energy values were calculated by a complete analysis of the population. The chemical hardness, electronegativity, electrophilicity, and chemical potential values were obtained to have information about the activity of the cluster by using the following equations. ϵ_{HOMO} is the highest occupied molecular orbital energy, and

ϵ_{LUMO} is the lowest unoccupied molecular orbital energy. These equations based on the Koopman's approach [5–9] are given as follows.

$$Chemical\ hardness\ (\eta) = \frac{I - A}{2} \quad (4)$$

$$Chemical\ potential\ (\mu) = -\frac{I + A}{2} \quad (5)$$

$$Electronegativity\ (\lambda) = -\mu \quad (6)$$

$$Electrophilicity\ (\omega) = \frac{\mu^2}{2\eta} \quad (7)$$

where $I \cong -\epsilon_{HOMO}\ and\ A \cong -\epsilon_{LUMO}$

The electron density (ED) and electron localization function (ELF) distribution maps have been obtained by using Multiwfn software [10]. Moreover, NBO atomic charges of atoms were obtained by Natural Bond Orbital (NBO) analysis [11]. Natural Population Analysis (NPA) has been utilized to obtain occupation numbers of orbitals of metal atoms. Raman frequency and activity values have also been obtained by frequency calculation in Single Point Energy (SPE) calculation. The scaling factor [5] was used as 0.9613 for all frequency values to regenerate experimental basics.

The convergence criteria are $12x10^{-4}$ for gradients of root-mean-square (rms) displacement, $18x10^{-4}$ for max displacement, $3x10^{-4}$ for rms force and $45x10^{-5}$ for the max force for theoretical calculations utilized in this study. The theoretical methodology utilized here: Firstly, the Spin Multiplicity (SM) for the system including adsorbing molecule and the cluster has been determined by SPE calculations. SPEs were calculated for different numbers of SM for separate systems, and then the number of SM which gives the lowest energy based on SPE calculation was accepted to be the final SM number for the related system. Then, the adsorbing molecule (DMAB molecule here) and the cluster were structurally optimized by EG calculations. The following equation has been used in order to compute the relative energy values for calculations.

$$\Delta(E/H) = (E/H)_{System} - (E/H)_{Adsortive} - (E/H)_{Cluster} \quad (1)$$

Here, $(E/H)_{System}$ is the calculated energy for the optimized system which contains the geometries of the adsorbing molecule and the cluster, $(E/H)_{Adsorptive}$ is the calculated energy

for the adsorbing molecule, e.g. DMAB molecule and $(E/H)_{Cluster}$ is the calculated energy for the original cluster.

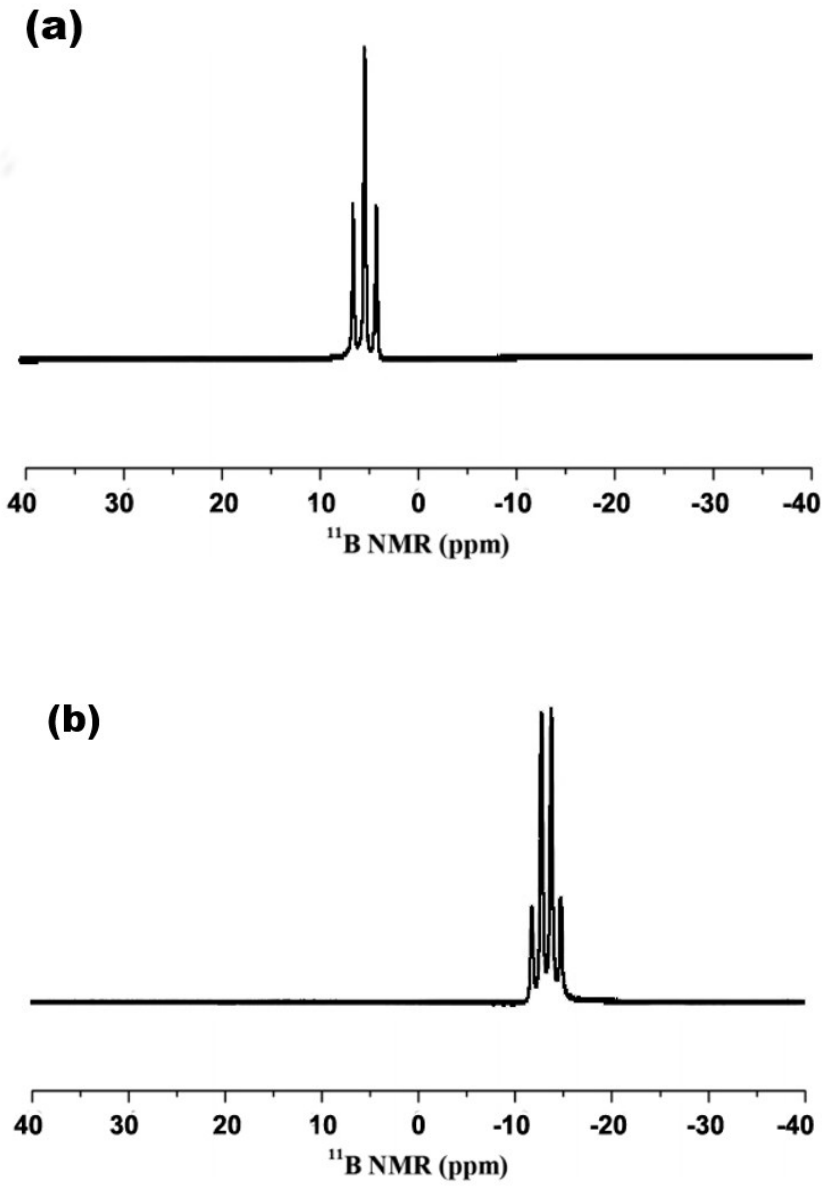

Figure S1. ^{11}B NMR spectra of (a) DMAB and (b) reaction solution taken at the end of the PtRh@GO catalyzed dehydrogenation of DMAB at room temperature.

Table S1: Turnover frequency values of catalysts for DMAB dehydrogenation

Entry	(Pre) Catalysts	Conv. (%)	Turnover Frequency (h^{-1})	Ea ($kJ.mol^{-1}$)	Temp. (°C)	Solvent	Ref.

1	**Graphene oxide based binary Platinum-Rhodium Nanomaterials**	**100**	**274.6**	**17**	**25**	**THF**	**This study**
2	Carbon black hybrid supported platinum nanomaterials	100	70.28	93.56	25	THF	[12]
3	Graphene oxide-based Palladium Nanoparticles	100	38.02	18.6	25	THF	[13]
4	Graphene oxide stabilized Palladium-Nickel Nanomaterials	100	271.90	38	25	THF	[14]
5	Ruthenium-based trimetallic nanomaterials	100	727	49.43	25	THF	[15]
6	Ruthenium-based complex	100	1.5	N/A	25	THF	[16]
7	Titanium-based complex	100	12.3	N/A	25	THF	[17]
8	Chromium-based complex	97	13.4	N/A	N/A	THF	[18]
9	Polymer-supported Ruthenium-Nickel Nanoparticles	100	458.57	36.52	N/A	THF	[19]
10	Nickel-based complex	100	3.2	N/A	20	THF	[20]
11	Rhodium-based complex	100	0.9	N/A	25	THF	[21]
12	TBA based Platinum nanoparticles	100	31.24	46.79	25	THF	[22]
13	Amylamine stabilized Platinum Nanoparticles	100	15.0	63.9	25	THF	[23]
14	PVP stabilized Palladium-Cobalt nanoparticles	100	330.94	50.78	25	THF	[24]
15	Ru0/APTS	100	55	61.1	25	THF	[25]
16	$Ru\ Cl_3.3H_2O$	77	2.7	N/A	25	THF	[25]
17	[Ru (1,5-cod) Cl_2]n	70	2.5	N/A	25	THF	[25]

18	PEDOT supported Palladium Nickel Nanoparticles	100	451.28	50.78	25	THF	[26]
19	Polymer-graphene based Platinum Nanomaterials	100	42.94	15.1	25	THF	[27]
20	Carbon-nanotube Based Ruthenium-cobalt nanoparticles	100	775.28	13.72	25	THF	[28]
21	RuCu@rGO	100	256.7	16.88	25	THF	[29]

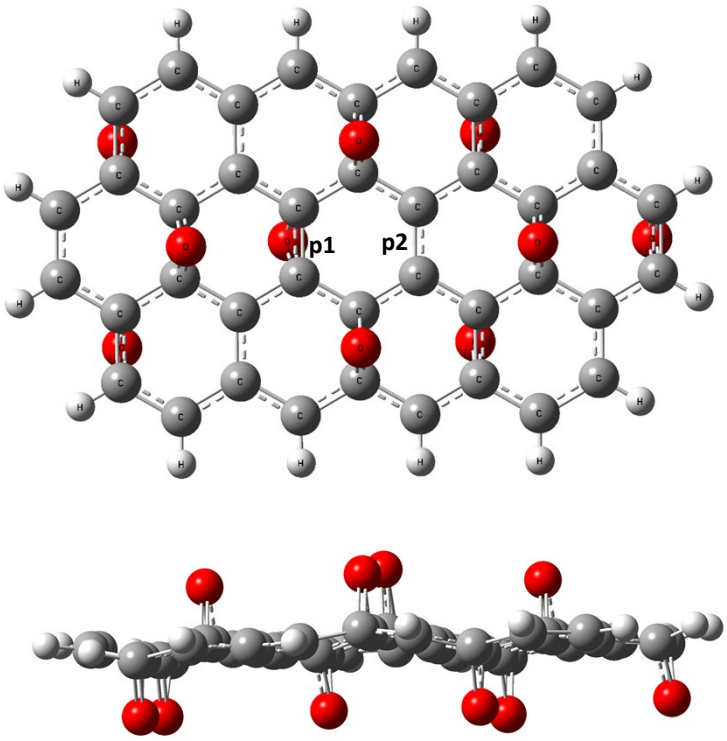

Figure S2. The optimized structure of GO cluster with top view and side view (p1 and p2 represent the possible position for the location of Pt and Rh atom.

Table S2. Energy values for optimized geometries of PtRh@GO cluster and PtRh@GO cluster with adsorbed DMAB molecule for location possibilities.				
	Locations of Pt and Rh atoms on p1 and p2 sites			
	PtRh@GO Cluster		PtRh@GO Cluster with adsorbed DMAB	
Energy Values (a.u.)	Rh-Pt	Pt-Rh	Rh-BMAB	Pt-BMAB
Sum of electronic and thermal Energies (E)	-2513.526198	**-2513.548457**	-2675.03883	**-2675.33997**
Sum of electronic and thermal Enthalpies (H)	-2513.525254	**-2513.547513**	-2675.302939	**-2675.339026**
Sum of electronic and thermal Free Energies (G)	-2513.627709	**-2513.648351**	-2675.419553	**-2675.455122**

References

S1. Shahriary, L. & Athawale, A. A. *Graphene Oxide Synthesized by using Modified Hummers Approach*. *International Journal of Renewable Energy and Environmental Engineering* **02**, (2014).

2. Wu, S.-Y., Lin, C.-H. & Ho, J.-J. Density-functional calculations of the conversion of methane to methanol on platinum-decorated sheets of graphene oxide. *Phys. Chem. Chem. Phys.* **17**, 26191–26197 (2015).

3. Frisch, M. J. *et al.* Gaussian09 Revision D.01, Gaussian Inc. Wallingford CT. *Gaussian 09 Revision C.01* (2010).

4. Foresman, J. & Frisch, A. Exploring chemistry with electronic structure methods, 1996 For Gaussian. *Gaussian Inc, Pittsburgh, PA* (1996).

5. Wong, M. W. Vibrational frequency prediction using density functional theory. *Chem. Phys. Lett.* **256**, 391–399 (1996).

6. Pearson, R. G. Chemical hardness and density functional theory. *J. Chem. Sci.* **117**, 369–377 (2005).

7. Suárez-Varela, J., Sakiyama, H., Cano, J. & Colacio, E. Interplay between covalent and aurophilic interactions in a series of isostructural 3D Hoffman-like frameworks

containing bipyrimidine and dicyanoaurate bridges. X-Ray structure and magnetic properties of {(μ-Au(CN) $_2$] $_2$ [(M(NH $_3$) $_2$) $_2$ (μ-bpym)]}[Au(CN) $_2$] $_2$ (M = Ni(ii), Co(ii) and Cu(ii)). *Dalt. Trans.* **0**, 249–256 (2007).

8. Parr, R. G. Density Functional Theory of Atoms and Molecules. in *Horizons of Quantum Chemistry* 5–15 (Springer Netherlands, 1980). doi:10.1007/978-94-009-9027-2_2

9. Pearson, R. G. The electronic chemical potential and chemical hardness. *J. Mol. Struct. THEOCHEM* **255**, 261–270 (1992).

10. Lu, T. & Chen, F. Multiwfn: A multifunctional wavefunction analyzer. *J. Comput. Chem.* **33**, 580–592 (2012).

11. Glendening, E. D., Badenhoop, J. K., Reed, A. D., Carpenter, J. E. & Weinhold, F. NBO 3.1. *Theor. Chem. Institute, Univ. Wisconsin, Madison, WI* (1990).

12. Sen, B., Şavk, A. & Sen, F. Highly efficient monodisperse Pt nanoparticles confined in the carbon black hybrid material for hydrogen liberation. *J. Colloid Interface Sci.* **520**, 112–118 (2018).

13. Şen, B. *et al.* Monodisperse palladium nanoparticles assembled on graphene oxide with the high catalytic activity and reusability in the dehydrogenation of dimethylamine-borane. *Int. J. Hydrogen Energy* **43**, 20176–20182 (2018).

14. Sen, B., Kuzu, S., Demir, E., Akocak, S. & Sen, F. Monodisperse palladium–nickel alloy nanoparticles assembled on graphene oxide with the high catalytic activity and reusability in the dehydrogenation of dimethylamine–borane. *Int. J. Hydrogen Energy* **42**, 23276–23283 (2017).

15. Sen, B., Kuzu, S., Demir, E., Onal Okyay, T. & Sen, F. Hydrogen liberation from the dehydrocoupling of dimethylamine–borane at room temperature by using novel and highly monodispersed RuPtNi nanocatalysts decorated with graphene oxide. *Int. J. Hydrogen Energy* (2017). doi:10.1016/j.ijhydene.2017.04.213

16. Friedrich, A., Drees, M. & Schneider, S. Ruthenium-Catalyzed Dimethylamineborane Dehydrogenation: Stepwise Metal-Centered Dehydrocyclization. *Chem. - A Eur. J.* **15**, 10339–10342 (2009).

17. Sloan, M. E. *et al.* Homogeneous Catalytic Dehydrocoupling/Dehydrogenation of

Amine−Borane Adducts by Early Transition Metal, Group 4 Metallocene Complexes. *J. Am. Chem. Soc.* **132**, 3831–3841 (2010).

18. Kawano, Y. *et al.* Dehydrocoupling Reactions of Borane−Secondary and −Primary Amine Adducts Catalyzed by Group-6 Carbonyl Complexes: Formation of Aminoboranes and Borazines. *J. Am. Chem. Soc.* **131**, 14946–14957 (2009).

19. Sen, B. *et al.* Highly efficient polymer supported monodisperse ruthenium-nickel nanocomposites for dehydrocoupling of dimethylamine borane. *J. Colloid Interface Sci.* (2018). doi:10.1016/j.jcis.2018.05.021

20. Robertson, A. P. M., Suter, R., Chabanne, L., Whittell, G. R. & Manners, I. Heterogeneous Dehydrocoupling of Amine–Borane Adducts by Skeletal Nickel Catalysts. *Inorg. Chem.* **50**, 12680–12691 (2011).

21. Jaska, C. A., Temple, K., Lough, A. J. & Manners, I. Transition metal-catalyzed formation of boron-nitrogen bonds: Catalytic dehydrocoupling of amine-borane adducts to form aminoboranes and borazines. *J. Am. Chem. Soc.* (2003). doi:10.1021/ja030160l

22. Erken, E. *et al.* New Pt(0) Nanoparticles as Highly Active and Reusable Catalysts in the C1–C3 Alcohol Oxidation and the Room Temperature Dehydrocoupling of Dimethylamine-Borane (DMAB). *J. Clust. Sci.* **27**, 9–23 (2016).

23. Sen, F., Karatas, Y., Gulcan, M. & Zahmakiran, M. Amylamine stabilized platinum(0) nanoparticles: active and reusable nanocatalyst in the room temperature dehydrogenation of dimethylamine-borane. *RSC Adv.* **4**, 1526–1531 (2014).

24. Çelik, B. *et al.* Monodispersed palladium–cobalt alloy nanoparticles assembled on poly(N-vinyl-pyrrolidone) (PVP) as a highly effective catalyst for dimethylamine borane (DMAB) dehydrocoupling. *RSC Adv.* **6**, 24097–24102 (2016).

25. Zahmakiran, M., Philippot, K., Özkar, S. & Chaudret, B. Size-controllable APTS stabilized ruthenium(0) nanoparticles catalyst for the dehydrogenation of dimethylamine-borane at room temperature. *Dalt. Trans.* (2012). doi:10.1039/c1dt11290b

26. Sen, B., Kuzu, S., Demir, E., Yıldırır, E. & Sen, F. Highly efficient catalytic dehydrogenation of dimethyl ammonia borane via monodisperse palladium–nickel

alloy nanoparticles assembled on PEDOT. *Int. J. Hydrogen Energy* **42**, 23307–23314 (2017).

27. Sen, B., Kuzu, S., Demir, E., Akocak, S. & Sen, F. Polymer-graphene hybride decorated Pt nanoparticles as highly efficient and reusable catalyst for the dehydrogenation of dimethylamine–borane at room temperature. *Int. J. Hydrogen Energy* **42**, 23284–23291 (2017).

28. Sen, B., Kuzu, S., Demir, E., Akocak, S. & Sen, F. Highly monodisperse RuCo nanoparticles decorated on functionalized multiwalled carbon nanotube with the highest observed catalytic activity in the dehydrogenation of dimethylamine−borane. *Int. J. Hydrogen Energy* **42**, 23292–23298 (2017).

29. Sen, B. *et al.* Monodisperse ruthenium–copper alloy nanoparticles decorated on reduced graphene oxide for dehydrogenation of DMAB. *Int. J. Hydrogen Energy* (2019). doi:10.1016/j.ijhydene.2019.02.176